Magnetic modulation of the tunneling between defects states in antidot superlattices

J.L. Movilla and J. Planelles

Departament de Química Física i Analítica, Universitat Jaume I, E-12080, Castelló, Spain

E-mail: josep.planelles@qfa.uji.es

Abstract. We show theoretically that the tunneling between properly designed defects in periodic antidot lattices can be strongly modulated by applied magnetic fields. Further, transport channels made up of linear arrangements of tunnel-coupled defects can accomodate Aharonov-Bohm cages, suggesting a magnetic control of the transport through the system. Evidence supporting an unusual robustness of the caging effect against electron-electron interactions is also provided.

PACS numbers: 73.22.-f, 73.21.Cd, 73.23.-b

Submitted to: *J. Phys.: Condens. Matter*

1. Introduction

Over the last two decades much attention has been paid to the physics of periodic structures imposed onto the plane of the two-dimensional electron system (2DES), and particularly to the quantum interference phenomena yielded by applied magnetic fields and the way in which they modulate their energy structure and related transport properties [1, 2, 3, 4, 5, 6, 7, 8, 9, 10, 11, 12, 13, 14, 15, 16]. Prompted by the advantages of the two-dimensional antidot lattices routinely fabricated nowadays, a new structure was proposed recently which seems to offer many attractive features in terms of flexibility, scalability, and operation in the pursuit of achieving solid-state quantum computation. Such scheme is based on quantum-mechanical bound states which form at designed defects in an antidot superlattice defined on a semiconductor heterostructure [17, 18, 19] or on a graphene sheet [20].

A missing antidot in the lattice leads to the formation of a quantum dot with a number of localized energy levels residing at the location of the defect that depends on the characteristic ratio between the antidot radius and the lattice constant. Similarly to conventional gate-defined double dot systems, the localized lowest-lying states corresponding to closely situated defects in the lattice can hybridize to form bonding and anti-bonding molecular states, a key feature to turn the system into a suitable candidate for quantum information processing in the solid state. The strength of the tunnel coupling between nearby defects (and hence the splitting between the lowest-lying molecular states) can be controlled by using a metallic split-gate defined on top of the 2DES, which constrains at will the connection between the defects by means of an applied voltage. The same tuning capability applies to the exchange coupling between the spins of electrons located in neighbouring defects [18].

In this paper we address the effects of an applied magnetic field on the electronic states ascribed to defects designed on an antidot lattice. By means of a numerically exact approach we first show that the Aharonov-Bohm-type quantum interferences can exert a strong influence over the tunnel coupling between nearby defects. Next we tackle the study of linear chains of coupled defects, which can constitute quantum channels along which magnetically controllable transport of electrons can take place. By using a simplified tight-binding model we show that such a quasi-one-dimensional lattice can accommodate AB cages [21, 22, 23, 24], which, interestingly, turn out to be unusually robust against electron-electron interactions.

2. Model

We consider a square lattice of antidots defined on a high-mobility two-dimensional electron system (2DES) such as a GaAs/GaAlAs semiconductor heterostructure. As in [16], the antidots are constituted by circular nanoholes practised in the 2DES that act as potential pillars for the electrons. Two or more defects are designed in the lattice in the form of absent holes. A portion of the resulting structure can be seen schematically

in figure 1(a).

In the effective mass approximation, the two-dimensional single-electron Schrödinger equation under a magnetic field perpendicular to the 2DES reads, in atomic units (a.u.),

$$H = \frac{1}{2m}(\mathbf{p} + \mathbf{A}(x, y))^2 + V(x, y). \tag{1}$$

In (1), m is the electron effective mass, and V is the potential modulation defining the hole lattice. Since the holes (of radius a and forming a square pattern of period L) constitute forbidden regions for the electrons, we set $V = \infty$ within a hole and $V = 0$ elsewhere. $\mathbf{A}$ is the potential vector defining the perpendicular magnetic field. In order to underscore the quantum-mechanical origin of the results and to favor the comparison with tight-binding approaches, we opted, as in [16], for a configuration such that the magnetic field pierces the system through the nanoholes only. With this arrangement, the magnetic field does not influence directly the electron motion, and thus the reported phenomenology is clearly non-classical in nature. $\mathbf{A}$ can be built then as the superposition of individual potential vectors, each defining a magnetic tube threading a flux Φ through a different hole of the lattice [16].

The eigenvalue equation of the Hamiltonian (1) is solved numerically using the finite difference method in a two-dimensional grid mapped in a finite region of the xy plane where defects are located. Concerning boundary conditions, a zero value of the wave functions is imposed in the edges of the integration box when studying molecules of defects. Conversely, to address the study of linear chains of coupled defects, magnetotranslation operators commuting with (1) are used to impose periodic boundary conditions in the x direction [25]. Details on the construction of $\mathbf{A}$ as well as on the implementation of magnetotranslations can be found in [16].

3. Results and discussion

We start by assessing the effect of the magnetic field on the two lowest-lying states of the molecular system comprised by two tunnel-coupled defects in the lattice. As shown in figure 1(a), such states are bound states that form when removing two nearby holes (antidots) of the otherwise periodic lattice [26]. The defects that we consider are separated by a hole, the magnetic flux through it being responsible for relevant AB-type quantum interference phenomena that bring about a large variation of the coupling strength between the defects states. This is reflected in the splitting between the ground and first excited energy levels, depicted in figure 1(b) as a function of the reduced flux Φ/Φ_0 piercing each lattice hole. The coupling strength becomes maximum for integer fluxes (in units of the flux quantum), whereas for half integers the tunneling between the defects is completely impeded. From this it follows that AB quantum interferences in the system can become fully destructive. It is worth stressing that, though not surprising, this result is far from obvious, since paths connecting the two defects others than those circumventing the intermediate hole are still available [27].

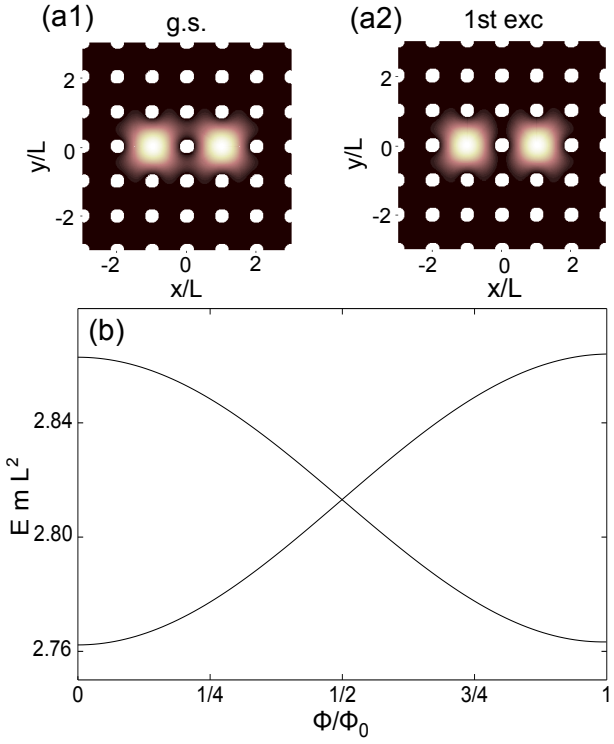

Figure 1. (a) Zero-field electron density distribution in the lowest-lying states of an antidot lattice with two tunnel-coupled defects separated by one antidot. The L/a ratio has been set to 16/3. (b) Corresponding energy of the two lowest-lying states as a function of the reduced flux threading each hole of the lattice. The spectrum exhibits the expected oscillatory behaviour, repeated indefinitely in the flux axis in units of one flux quantum.

Note also that the represented spectrum is approximately symmetric in the energy axis. The interaction with upper states is the reason for the slight deviation from the perfect symmetry, which is attained gradually as the ratio L/a diminishes (not shown).

The feasibility of the gate control of the tunneling between defects raised the perspective, in view of potential quantum information applications, of designing architectures consisting of antidot lattices with linear arrays of defect states constituting quantum channels along which coherent and controllable transport could take place [18]. Similarly, the large degree of magnetic control over the tunneling reported in figure 1, together with the exotic and rich behaviour of antidot lattices under applied magnetic fields, prompts us to turn the attention to the periodic counterpart of the coupling between defects, and the way in which the external field modulates the pattern of minibands that show up in the spectrum.

Figure 2 shows the low energy range of the miniband spectrum for different configurations of the linear array of defects sketched in 2(a). The represented region is energetically distant from more excited minibands and, particularly, from the butterfly-type spectrum of the hosting antidot lattice. As can be seen, the complexity of the spectrum (though also the versatility of the system, as will be shown later) can be

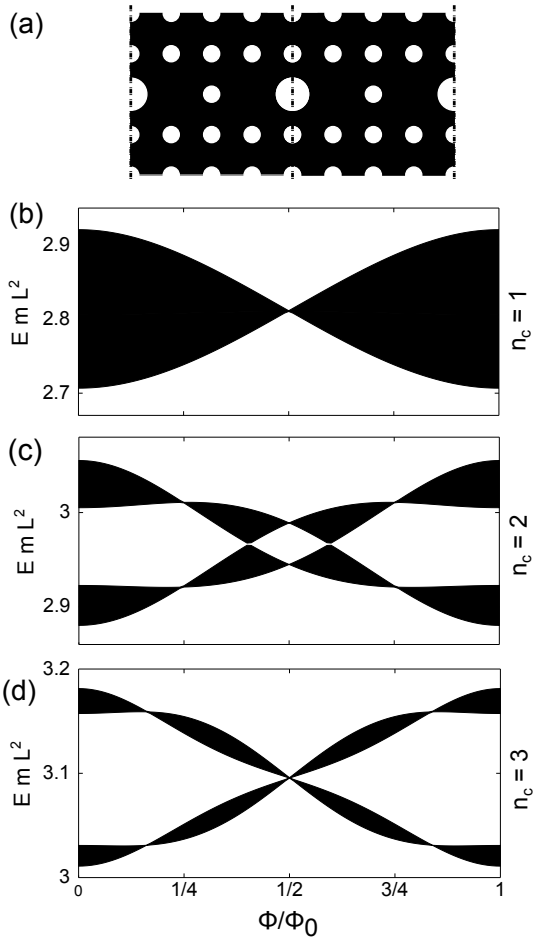

Figure 2. (a) Schematics of the linear arrays of defects studied. The defects are separated alternatively by holes of two different sizes, n_c being the ratio between their areas. (b)-(d) Low energy range of the miniband structures calculated for $n_c = 1$, 2, and 3, respectively, depicted as a function of the magnetic flux Φ/Φ_0 threading each of the smaller holes of the array. The magnetic field piercing holes of different area is assumed to be the same, so the corresponding fluxes differ by a factor n_c. Black areas correspond to permitted energies.

manipulated through the design of the lattice. Thus, on panels 2(c) and 2(d) the defects are separated alternatively by holes of two different sizes (n_c being the ratio between their area), which modifies qualitatively the spectrum due mainly to two reasons: (i) two different magnitudes of the tunnel coupling strength are present (holes with larger/smaller area yield a smaller/larger constriction of the tunneling between the adjacent defects), and (ii) the magnetic flux through the two kinds of holes also differ, which generates a double pattern of AB-type quantum interferences in the lattice. In all cases one can see that the bandwidth is strongly modulated by the magnetic flux, to the point that flat band conditions are achieved for particular values of the field. These values are those fulfilling that the flux through any of the two types of holes equals a half integer in units of the flux quantum Φ_0. In units of the reduced flux through the smaller

hole, Φ/Φ_0, this occurs when $\Phi/\Phi_0 = \frac{2n+1}{2}$ and $\Phi/\Phi_0 = \frac{2n+1}{2n_c}$, with $n = 0, 1, 2, \ldots$

As we will show later, a flat band spectrum reflects the appearance of bound Aharonov-Bohm cages in the system. The AB caging effect, first predicted by Vidal *et al.* [21], is an extreme localization phenomenon originated from a subtle interplay between the geometry of bipartite lattices and quantum interferences of an AB type, which become fully destructive for particular values of the field. This interplay bounds the set of sites eventually visited by an initially localized wave packet, thus localizing non-interacting electrons in finite regions of the lattice termed AB cages.

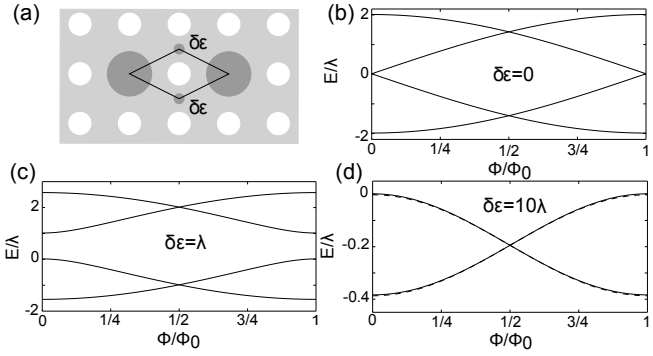

Figure 3. (a) Diamond-like tight-binding scheme connecting two adjacent defects. Top and bottom centres can be subjected to additional on-site potentials $\delta\epsilon$. (b)-(d) Corresponding low-lying energy spectra vs. the reduced flux obtained for different values of $\delta\epsilon$ (solid lines). The dashed lines in (d) correspond to the approximation given by (3).

To gain insight into the dynamical aspects of this phenomenon in our system, we introduce next a simplified, one-dimensional tight-binding (TB) description of the linear array of defects. To this aim, we shall model the coupling between two adjacent defects by means of a field-dependent, effective hopping parameter capable of reproducing the energy spectrum and, particularly, the fully destructive interferences yielded by the magnetic field at specific values. To obtain such an effective parameter we depart from the well-known diamond-like TB structure depicted in figure 3(a), where the upper and lower sites may be subject to an additional on-site potential $\delta\epsilon$. Figure 3(b)-(d) show the corresponding energy spectra calculated in the nearest-neighbour approach for increasing values of $\delta\epsilon$. Under large on-site potentials [Figure 3(d)], the low-lying spectrum of the TB structure mimics accurately that of the coupled defects of figure 1(b), which can be rationalized from the fact that defects states are expected to be much more stable than those associated to the inter-hole spacing [see figure 3(a)].

The simplicity of the diamond-like TB model allows us to diagonalize analytically the corresponding hamiltonian matrix. The energy obtained for the two lowest-lying molecular levels is given by

$$E_{\pm} = \frac{\delta\epsilon}{2} - \frac{1}{2}\sqrt{\delta\epsilon^2 + 8\lambda^2(1 \pm \cos\pi\frac{\Phi}{\Phi_0})}, \tag{2}$$

where λ stands for the zero-field tunnel matrix element and Φ/Φ_0 is the reduced flux threading the rhombus. For large values of $\delta\epsilon/\lambda$, the series expansion of (2) in terms of $\cos\pi\frac{\Phi}{\Phi_0}$ can be safely truncated in the linear term, yielding

$$E_{\pm} \approx \frac{1}{2}\left(\delta\epsilon - \lambda\sqrt{8+(\delta\epsilon/\lambda)^2}\right) \mp \frac{2\lambda}{\sqrt{8+(\delta\epsilon/\lambda)^2}}\cos\pi\frac{\Phi}{\Phi_0}. \tag{3}$$

The accuracy of this approximation is illustrated in figure 3(d), where the energy levels estimated by (3) are also represented (dashed lines). From (3) follows that the effective hopping parameter between the two defects results $\lambda^{eff} = 2\lambda(8 + \delta^2/\lambda^2)^{-1/2}\cos\pi\Phi/\Phi_0$.

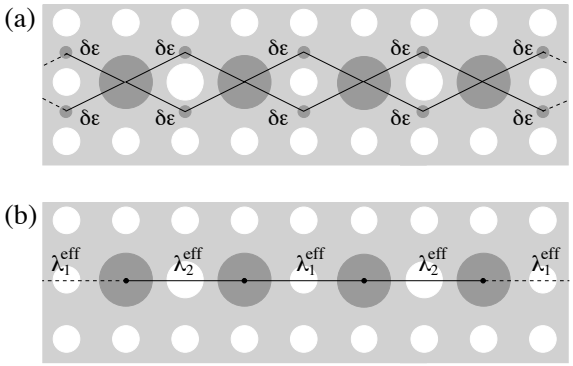

Figure 4. Schematics of the two tight-binding approaches employed to describe the linear arrays of defects: (a) Diamond chain subject to additional on-site potentials $\delta\epsilon$ on edge centres (small, dark-grey circles). (b) Simplified, one-dimensional model connecting adjacent defects (large, dark-grey circles) by means of an effective hopping parameter $\lambda^{eff} = 2\lambda(8 + \delta^2/\lambda^2)^{-1/2}\cos\pi\Phi/\Phi_0$, where Φ/Φ_0 stands for the magnetic flux quanta threading the hole between the connected defects and λ is the zero-field tunnel matrix element corresponding to the diamond chain model. Under large $\delta\epsilon$ values both approaches converge, and successfully describe the low-lying region of the spectrum.

The field-dependent behaviour of the linear arrays of defects shown in figure 2 can also be reproduced accurately -up to a zero energy offset- by using a simplified, one-dimensional TB model (see figure 4) which considers only sites located at the defects and connected by means of this effective hopping parameter. This can be seen in figure 5, where different energy spectra are represented for the periodic counterpart of the diamond-like TB structure (both with and without large on-site potentials), as well as for the simplified one-dimensional TB model. In the diamond-like simulations with $n_c \neq 1$ (two lower panels of the left and central columns), two different values of the zero-field tunnel-coupling strength (λ and $\lambda/2$) have been employed in order to emulate the different constriction of the tunneling around different hole sizes. As a result, the effective coupling between adjacent defects derived for the one-dimensional TB scheme alternates between $\lambda_1^{eff} = 2\lambda(8 + \delta\epsilon^2/\lambda^2)^{-1/2}\cos\pi\Phi/\Phi_0$ and $\lambda_2^{eff} = \lambda(8 + 4\delta\epsilon^2/\lambda^2)^{-1/2}\cos n_c\pi\Phi/\Phi_0$, where, as in figure 2, Φ/Φ_0 stands for the

reduced flux through each of the holes with smaller area. Note the different argument of the cosine in λ_1^{eff} and λ_2^{eff}, which is a consequence of the different phase accumulated by the electron when circumventing holes of different area.

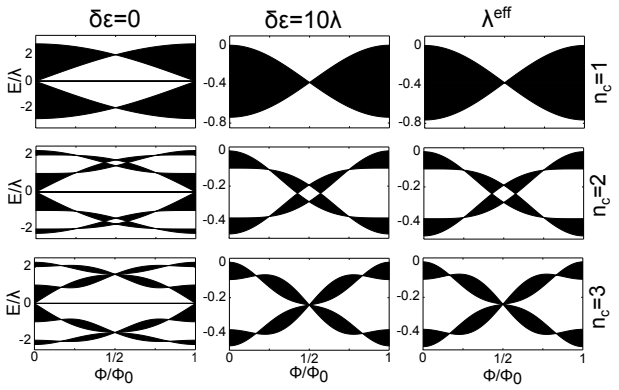

Figure 5. Miniband structures calculated for the same systems as in figure 2 but using tight-binding models. Left and central column panels: Diamond-like tight-binding model with $\delta\epsilon = 0$ and 10λ, respectively. In the last case only the low-lying region of the spectrum is represented [28]. Right column panels: Simplified one-dimensional tight-binding model with $\delta\epsilon = 10\lambda$. An energy offset has been included in this last case to facilitate the comparison with the diamond-like tight-binding results of the central column.

A straightforward analysis reveals that, for rational values of $n_c = p/q$, with p and q integers and relative prime, the spectrum exhibits a periodicity q in the flux axis. In such a period, λ_1^{eff} (λ_2^{eff}) is cancelled q (p) times, specifically when Φ/Φ_0 equals $\frac{2n-1}{2}$ ($\frac{2n-1}{2}\frac{q}{p}$), with $n = 1, \ldots, q$ ($n = 1, \ldots, p$). For these flux values, the tunneling between the corresponding defects is totally impeded, the miniband structure becomes flat, and bound AB cages form in the structure. We illustrate this phenomenon by wave packet propagations: An electron initially prepared in the central site of a finite but large array of defects is left to evolve coherently through the lattice, and its propagation is monitored by plotting the overlap of the time-dependent wave function with the initial state. The results are collected in figure 6 for $n_c = 8/3$ and different magnetic fluxes.

One can observe that (i) for most (non-specific) flux values [see figure 6(a)], there is a double modulation of the occupation probability of the initial site, characterized by an overall gradual attenuation that indicates the spreading of the electron through the lattice, (ii) in the conditions given by $\Phi/\Phi_0 = \frac{2n-1}{2}$ and $\Phi/\Phi_0 = \frac{2n-1}{2}\frac{q}{p}$, $n = 1, 2, \ldots$ (for which the spectrum becomes flat), the overlap displays regular, non-attenuated sinusoidal oscillations [figures 6(b) and 6(c)], indicating that the electron density is trapped in an AB cage constituted by two adjacent defects between which it oscillates periodically, and (iii) the timescale of such an intra-cage oscillation varies strongly depending on the selected flux; the corresponding period T_i ($= \pi/|\lambda_i^{eff}|$) can be estimated by $T_1 = \pi(8 + \delta\epsilon^2/\lambda^2)^{1/2} \left|2\lambda \cos\left(\pi \frac{2n-1}{2}\frac{q}{p}\right)\right|^{-1}$ ($n = 1, \ldots, p$) for fluxes yielding $\lambda_2^{eff} = 0$, and by $T_2 = \pi(8 + 4\delta\epsilon^2/\lambda^2)^{1/2} \left|\lambda \cos\left(\pi \frac{2n-1}{2}\frac{p}{q}\right)\right|^{-1}$ ($n = 1, \ldots, q$) for $\lambda_1^{eff} = 0$

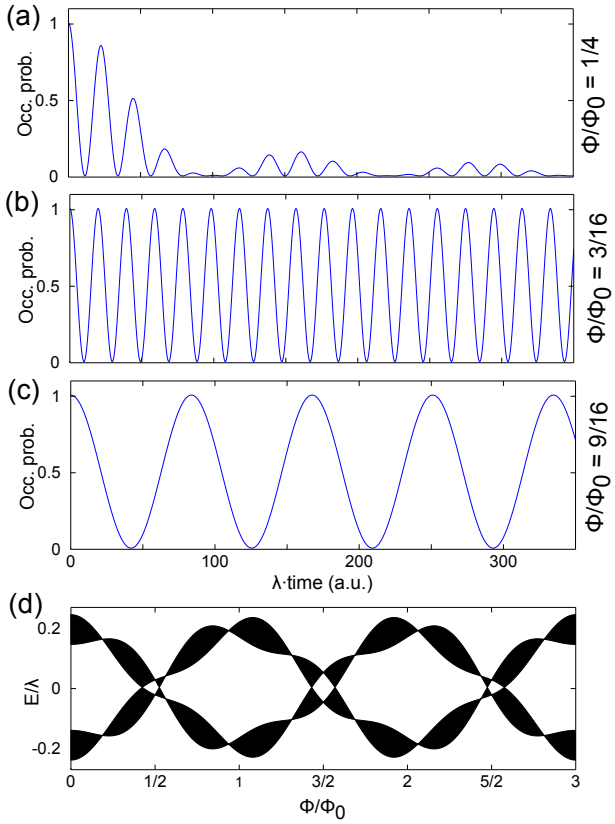

Figure 6. (a)-(c) Time-dependent occupation probability of the initial site for an electron evolving coherently in a finite array of defects modelled in the one-dimensional TB approach with $n_c = 8/3$. The array is large enough as to avoid the reflection of the wave packet with the edges in the illustrated timescales. (d) Corresponding miniband structure, calculated using the same parameters as in figure 5. The figure extends over one period in the flux axis.

fluxes. As a result, and taking symmetries into account, a total of up to $(p + q + 1)/2$ different periods can be selected for intra-cage oscillations, related to that many flux values. Departing from these values enables the electron transport through the lattice, in a timescale also dependent on the selected flux.

We shall discuss finally on the effect of the electron-electron interaction on the localization of many-electron wave-packets. AB cages in two-dimensional and quasi-one-dimensional bipartite lattices have been proven to be robust against a small but sizeable disorder and the presence of on-site potentials [29, 30, 31], but become rapidly unbound as soon as the electrons interact, owing to the generation of extended many-particle states [30, 32]. However, the close agreement between our numerical results and those derived from the one-dimensional TB model provides evidence that the localization phenomenon addressed here should persist in the presence of low or even moderate electron-electron interactions. Mathematically, this can be inferred from the fact that the effective hopping parameter λ^{eff} derived for the one-dimensional TB model is completely annulled for specific values of the flux. Indeed, within this

simplified, nearest-neighbour TB formalism, one easily realizes that the corresponding single-electron matrix representation becomes blocked for certain flux values, owing to the cancellation of the off-diagonal terms involving λ^{eff}. This clearly reflects the cage formation, since the sites in a given block can interact only among them. In the many-electron representation the scenario is essentially similar, since the Coulomb interaction terms are always diagonal regardless of the approximation assumed to describe them (Hubbard, extended Hubbard, or even Parisier-Parr-Popple [33]), and, in consequence, λ^{eff} is still the only off-diagonal source of coupling. When λ^{eff} cancels for certain fluxes, the Hamiltonian gets blocked, which translates into the impossibility for a many-electron wave-packet to extend beyond the block(s) initially occupied. The many-electron cage, understood as the set of sites visited by an initially localized many-electron packet, becomes thus bound.

Physically, the ultimate reason for this unusual lack of interaction-induced delocalization is the pronounced restriction that the geometry of the system exerts over those tunneling processes that involve the simultaneous hop of two electrons between adjacent defects. In the bipartite lattices that support AB cages studied so far, the mechanism responsible for the suppression of the localization effect involves the coordinated hop of two electrons between adjacent single-electron cages, a tunneling process which is allowed since it does not follow the same pattern of AB interferences as single electron ones [34, 35, 36, 37, 38]. However, by studying the two-electron dynamics in the quasi-one-dimensional diamond chain, we showed recently that the introduction of on-site potentials ($\delta\epsilon$) on the edge sites reduce noticeably the rate of two-electron hopping mechanisms as compared to single-electron ones, to the point of achieving an effective preservation of the AB cages in the system for large enough values of $\delta\epsilon$ [38]. The close correspondence established previously between the linear chain of defects in the antidot lattice and the diamond-like network with large on-site potentials on edge sites provides a physical understanding of the localization phenomenon in the presence of electron-electron interactions.

4. Conclusions

By means of both exact (numerical) and tight-binding approaches, we have shown that the quantum interferences of an Aharonov-Bohm type produced by an applied magnetic field can strongly modulate the tunnel coupling between defects in an antidot superlattice. The suitable arrangement of defects in linear chains generates a miniband pattern which is very sensitive to the field strength, and that becomes flat for certain values of the magnetic flux. This last feature is related to the formation of bound AB cages, which present evidence of being unusually robust against electron-electron interactions. The large degree of magnetic control over the coherent transport in these systems, which includes the possibility of isolating molecules of defects with the desired level structure (and thus dynamics timescales) despite electron-electron interactions, might be of practical interest for quantum computation purposes.

Acknowledgments

Support from MICINN project CTQ2011-27324 and UJI-Bancaixa projects P1-1A2009-03 and P1-1B2011-01 is acknowledged.

References

[1] Rössler U and Suhrke M 2000 Bloch electrons in a magnetic field: Hofstadter's butterfly *Advances in Solid State Physics* vol 40 ed Kramer B (Berlin: Springer) pp 35–50
[2] Springsguth D, Ketzmerick R and Geisel T 1997 *Phys. Rev. B* **56**(4) 2036–2043
[3] Schösser T, Ensslin K, Kotthaus J P and Holland M 1996 *Europhys. Lett.* **33** 683
[4] Albrecht C, Smet J H, von Klitzing K, Weiss D, Umansky V and Schweizer H 2001 *Phys. Rev. Lett.* **86**(1) 147–150
[5] Geisler M C, Smet J H, Umansky V, von Klitzing K, Naundorf B, Ketzmerick R and Schweizer H 2004 *Phys. Rev. Lett.* **92**(25) 256801
[6] Koshino M and Ando T 2004 *Journal of the Physical Society of Japan* **73** 3243–3246
[7] Kato M, Endo A, Katsumoto S and Iye Y 2008 *Phys. Rev. B* **77**(15) 155318
[8] Weiss D, Richter K, Menschig A, Bergmann R, Schweizer H, von Klitzing K and Weimann G 1993 *Phys. Rev. Lett.* **70**(26) 4118–4121
[9] Weiss D, Roukes M L, Menschig A, Grambow P, von Klitzing K and Weimann G 1991 *Phys. Rev. Lett.* **66**(21) 2790–2793
[10] Meckler S, Heinzel T, Cavanna A, Faini G, Gennser U and Mailly D 2005 *Phys. Rev. B* **72**(3) 035319
[11] Grant D E, Long A R and Davies J H 2000 *Phys. Rev. B* **61**(19) 13127–13130
[12] Yevtushenko O, Lütjering G, Weiss D and Richter K 2000 *Phys. Rev. Lett.* **84**(3) 542–545
[13] Wang X F, Vasilopoulos P and Peeters F M 2004 *Phys. Rev. B* **69**(3) 035331
[14] Khoury M, Lacasta A M, Sancho J M, Romero A H and Lindenberg K 2008 *Phys. Rev. B* **78**(15) 155433
[15] Wang X F, Vasilopoulos P and Peeters F M 2004 *Phys. Rev. B* **70**(15) 155312
[16] Movilla J L and Planelles J 2011 *Phys. Rev. B* **83**(1) 014410
[17] Flindt C, Mortensen N A and Jauho A P 2005 *Nano Letters* **5** 2515–2518
[18] Pedersen J, Flindt C, Asger Mortensen N and Jauho A P 2008 *Phys. Rev. B* **77**(4) 045325
[19] Pedersen J, Flindt C, Mortensen N A and Jauho A P 2008 *Physica E* **40** 1075 – 1077
[20] Pedersen T G, Flindt C, Pedersen J, Mortensen N A, Jauho A P and Pedersen K 2008 *Phys. Rev. Lett.* **100**(13) 136804
[21] Vidal J, Mosseri R and Douçot B 1998 *Phys. Rev. Lett.* **81**(26) 5888–5891
[22] Naud C, Faini G and Mailly D 2001 *Phys. Rev. Lett.* **86**(22) 5104–5107
[23] Pop I M, Hasselbach K, Buisson O, Guichard W, Pannetier B and Protopopov I 2008 *Phys. Rev. B* **78**(10) 104504
[24] Gladchenko S, Olaya D, Dupont-Ferrier E, Dou¸cot B, Ioffe L B and Gershenson M E 2009 *Nature Phys.* **5**(1) 48–53
[25] In this preliminary study we neglect the coupling to quantum lead contacts and the effect of disorder that could be present in concrete realizations of these systems.
[26] It has been proved that the corresponding eigenfunctions decay to zero within a finite distance from the defects, and that they are unaffected by increasing further the size of the integration box [see figure 1(a)].
[27] In the light of the results, these alternative paths are energetically inaccessible for electrons in the lowest-lying states.
[28] Note that, since the non-dispersive, flux-independent band characteristic of the diamond-like periodic structure is ascribed to edge sites, it moves to high energies when such centres are

subject to large, positive on-site potentials (see e.g. [39]). This is the reason why it does not show up in the central column panels of figure 5 ($\delta\epsilon = 10\lambda$), where only the low-lying region of the spectrum is represented.

[29] Vidal J, Montambaux G and Douçot B 2000 *Phys. Rev. B* **62**(24) R16294–R16297
[30] Vidal J, Butaud P, Douçot B and Mosseri R 2001 *Phys. Rev. B* **64**(15) 155306
[31] Oh G Y 2003 *J. Korean Phys. Soc.* **42**(5) 714–717
[32] Vidal J, Douçot B, Mosseri R and Butaud P 2000 *Phys. Rev. Lett.* **85**(18) 3906–3909
[33] Powell B J arXiv 0906.1640
[34] Kazymyrenko K, Dusuel S and Douçot B 2005 *Phys. Rev. B* **72**(23) 235114
[35] Douçot B and Vidal J 2002 *Phys. Rev. Lett.* **88**(22) 227005
[36] Souza D and Claro F 2010 *Phys. Rev. B* **82**(20) 205437
[37] Creffield C E and Platero G 2010 *Phys. Rev. Lett.* **105**(8) 086804
[38] Movilla J L and Planelles J 2011 *Phys. Rev. B* **84**(19) 195110
[39] Sil S, Maiti S K and Chakrabarti A 2009 *Phys. Rev. B* **79**(19) 193309